

## Observation of a Free-Shercliff-Layer Instability in Cylindrical Geometry

Austin H. Roach,<sup>\*</sup> Erik J. Spence, Christophe Gissinger, Eric M. Edlund,  
Peter Sloboda, Jeremy Goodman, and Hantao Ji<sup>†</sup>

*Center for Magnetic Self-Organization in Laboratory and Astrophysical Plasmas and Princeton Plasma Physics Laboratory,  
P.O. Box 451 Princeton, New Jersey 08543, USA*

(Received 16 December 2011; published 11 April 2012)

We report on observations of a free-Shercliff-layer instability in a Taylor-Couette experiment using a liquid metal over a wide range of Reynolds numbers,  $Re \sim 10^3$ – $10^6$ . The free Shercliff layer is formed by imposing a sufficiently strong axial magnetic field across a pair of differentially rotating axial end cap rings. This layer is destabilized by a hydrodynamic Kelvin-Helmholtz-type instability, characterized by velocity fluctuations in the  $r$ - $\theta$  plane. The instability appears with an Elsasser number above unity, and saturates with an azimuthal mode number  $m$  which increases with the Elsasser number. Measurements of the structure agree well with 2D global linear mode analyses and 3D global nonlinear simulations. These observations have implications for a range of rotating MHD systems in which similar shear layers may be produced.

DOI: [10.1103/PhysRevLett.108.154502](https://doi.org/10.1103/PhysRevLett.108.154502)

PACS numbers: 47.65.-d, 47.15.St, 47.20.Ft

The destabilization of rotating sheared flows by an applied magnetic field in magnetohydrodynamics (MHD) is a topic with astrophysical and geophysical implications, and has been the subject of a number of experimental and theoretical efforts. Such destabilization can be caused by the magnetorotational instability (MRI), in which a magnetic field of sufficient amplitude can destabilize Rayleigh-stable rotating sheared flows [1]. In this Letter, we report the observation of an instability which, like the MRI, appears in a sheared rotating fluid when a magnetic field is applied. But rather than playing a role in the dynamics of the instability, as in the case of the MRI, the magnetic field here acts to establish free shear layers which extend from axial boundaries and which are subject to a hydrodynamic instability.

Hartmann and Shercliff laid the groundwork in understanding the effect of magnetic fields on shear layers in conducting fluids. Hartmann studied boundary layers normal to an external applied field [2], and Shercliff extended his analysis to include boundary layers parallel to the applied field [3]. Free Shercliff layers can be established in rotating MHD systems when the line-tying force of an axial magnetic field extends a discontinuity in angular velocity at an axial boundary into the bulk of the fluid. These shear layers are similar to the Stewartson layers that extend from discontinuous shearing boundaries in rapidly rotating systems [4], but for the free Shercliff layer discussed here, it is the magnetic field tension rather than the Coriolis force that leads to equalization of the angular velocity in the axial direction.

Free Shercliff layers were first realized experimentally by Lehnert in a cylindrical apparatus with a free surface at the top and a rotating ring at the bottom axial boundary [5]. Lehnert observed the formation of vortices at the location of the shear layers, though he attributed their formation to

discontinuities in the free surface at the shear layer location rather than to the shear itself. These layers were then described analytically by Stewartson [6] and Braginskii [7]. The formation of free Shercliff layers in a cylindrical Taylor-Couette device has been predicted computationally [8], but these simulations were axisymmetric and thus incapable of evaluating the stability of these shear layers to nonaxisymmetric perturbations.

Both free Shercliff layers and Stewartson layers can be present at the tangent cylinder of spherical Couette systems. The Kelvin-Helmholtz destabilization of these layers has been studied extensively through computation [9–11]. Stewartson layers have been observed experimentally in spherical and cylindrical geometry and are found to be unstable to nonaxisymmetric modes, which is consistent with simulations [10,12,13].

The Princeton MRI experiment is a Taylor-Couette apparatus consisting of two coaxial stainless steel cylinders as shown in Fig. 1. The gap between the cylinders is filled with a GaInSn eutectic alloy which is liquid at room temperature. Differential rotation of the cylinders sets up a sheared rotation profile in the fluid. If the cylinders were infinitely long, the fluid between the cylinders would assume an angular velocity  $\Omega$  at a radius  $r$  matching the ideal Couette solution in steady state,  $\Omega(r) = a + b/r^2$ . The constants  $a$  and  $b$  are found by matching the solution to the imposed rotation rates at the inner and outer cylinder boundaries. In conventional Taylor-Couette devices, the end caps are typically corotated either with the inner or outer cylinder. This produces strong secondary circulation and angular momentum transport to the axial boundaries, resulting in a deviation from the ideal rotation profile [14]. A novelty of this apparatus is the configuration of the axial end caps, each of which is split into two differentially rotatable acrylic rings, giving four independent rotation

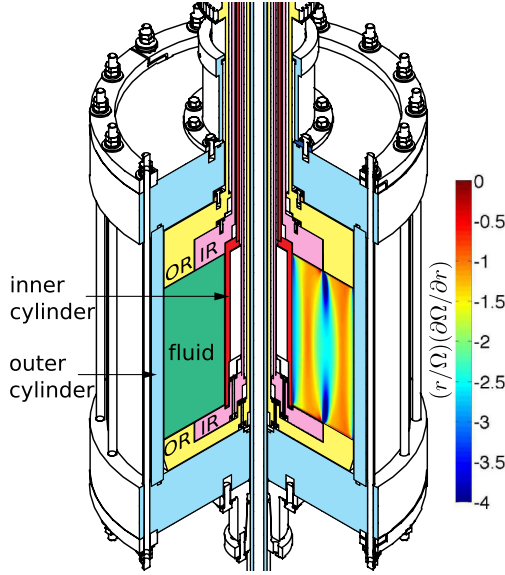


FIG. 1 (color online). Diagram of Princeton MRI experiment. Each end cap is split into an inner ring (IR) and an outer ring (OR). Differential rotation of these rings produces a discontinuity in the angular velocity at the axial boundary. Overlaid on the right half of the figure is a plot of the shear  $(r/\Omega)(\partial\Omega/\partial r)$  from a nonlinear MHD simulation with differential rotation between the end cap rings and a strong axial magnetic field [21]. The free Shercliff layers are the regions of strong negative shear extending from the interface between the rings.

rates: those of the inner cylinder, outer cylinder, inner rings, and outer rings. In previous experiments using water as the working fluid, this configuration was very effective at reducing the influence of the axial boundaries, allowing the generation of quiescent flows in the bulk of the fluid with Reynolds numbers  $Re = \Omega_1 r_1 (r_2 - r_1) / \nu$  above  $10^6$  [15]. The experimental parameters are shown in Table I.

Fluid velocities are measured with an ultrasound Doppler velocimetry (UDV) system [18,19]. Ultrasonic transducers are mounted on the outer cylinder at the mid-plane of the experiment. A transducer aimed radially and others aimed tangential to the inner cylinder allow determination of the radial and azimuthal velocity components. Two tangential transducers aimed identically but separated

TABLE I. Parameters of the apparatus [16] and liquid metal working fluid [17].

Parameter	symbol	value	units
Height	$h$	27.9	cm
Inner cylinder radius	$r_1$	7.06	cm
Outer cylinder radius	$r_2$	20.3	cm
Density	$\rho$	6.36	$\text{g/cm}^3$
Kinematic viscosity	$\nu$	$2.98 \times 10^{-3}$	$\text{cm}^2/\text{s}$
Magnetic diffusivity	$\eta$	$2.57 \times 10^3$	$\text{cm}^2/\text{s}$
Inner cylinder rotation rate	$\Omega_1$	0.25–800	rpm
Axial magnetic field	$B$	0–4500	Gauss

azimuthally by  $90^\circ$  provide information about azimuthal mode structure.

A set of six solenoidal coils applies an axial magnetic field to the rotating fluid. Fields below 800 Gauss can be applied indefinitely, while the application time for higher fields is limited by the resistive heating of the coils. An array of 72 magnetic pickup coils placed beyond the outer cylinder measures  $\partial B_r / \partial t$ .

Experiments were run using both Rayleigh-stable and -unstable flow states. The Rayleigh-stable states had component rotation speeds in the ratio [1.0, 0.55, 0.1325, 0.1325] for the inner cylinder, inner ring, outer ring, and outer cylinder, respectively. The ideal Couette solution for these inner and outer cylinder speeds satisfies Rayleigh's stability criterion that the specific angular momentum increase with radius:  $\partial(r^2\Omega)/\partial r > 0$ . The ring speeds were chosen empirically to generate an azimuthal rotation profile in the hydrodynamic case that closely matches the ideal Couette profile at the midplane. The Rayleigh-unstable states were generated using component speeds in the ratio [1.0, 1.0, 0, 0]. These flows violate Rayleigh's criterion and exhibit large velocity fluctuations in the absence of a magnetic field.

A single run of this experiment starts with an acceleration phase of two minutes, during which the sheared azimuthal flow develops. The axial magnetic field is then applied, initially resulting in the damping of hydrodynamic fluctuations. If the magnetic field is strong enough to satisfy the requirement that the Elsasser number  $\Lambda = B^2 / 4\pi\rho\eta\Delta\Omega > 1$ , where  $\Delta\Omega$  is the difference between the inner- and outer-ring rotation rates, the instability grows up as a large-scale coherent mode. It manifests itself as a fluctuation in the radial velocity and azimuthal velocity, where significant perturbations of more than 10% of the inner cylinder speed are observed. An ultrasonic transducer inserted on a probe and aimed axially at an end cap did not measure axial velocity fluctuations when the instability was excited, suggesting that the flow due to the instability is mainly in the  $r$ - $\theta$  plane. Correlated magnetic fluctuations are observed at the highest rotation rates and applied fields. The instability develops on both the Rayleigh-stable and -unstable backgrounds, and typical mode rotation rates exceeds the outer cylinder rotation rate  $\Omega_2$  by  $\sim 0.1(\Omega_1 - \Omega_2)$ .

The instability was observed over a range of more than 3 orders of magnitude in rotation rate in the Rayleigh-unstable configuration, as shown in Fig. 2, with  $Re = 820 - 2.6 \times 10^6$ . The instability is present even with a magnetic Reynolds number  $Rm = \Omega_1 r_1 (r_2 - r_1) / \eta \sim 10^{-3}$ , indicating an inductionless mechanism in which induced magnetic fields are dynamically unimportant.

For  $\Lambda$  of order one, the primary azimuthal mode number at saturation is  $m = 1$ , with phase-locked higher-order mode numbers typically present at a smaller amplitude. The measured mode structure is shown in Fig. 3. It is

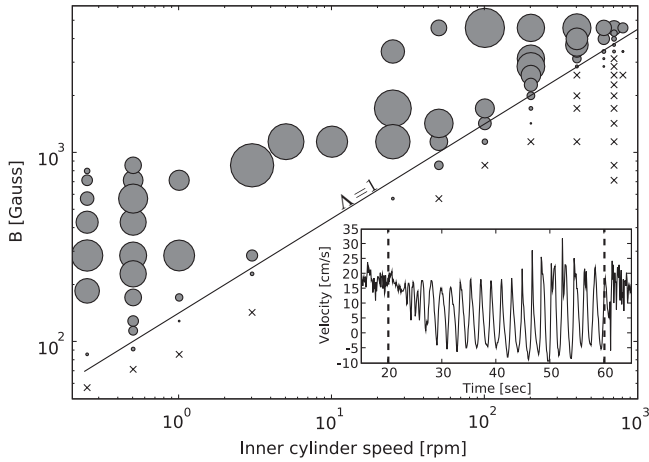


FIG. 2. Stability diagram for the Rayleigh-unstable background flow state. The area of the circles is proportional to the power in the dominant Fourier harmonic measured by a tangential transducer at  $r = 19.2$  cm, normalized to the square of the inner cylinder speed. The 'x's indicate stability. The stability diagram for the case starting from a Rayleigh-stable background is similar, but was measured over a smaller range of speeds. The inset plot shows a sample time trace of the velocity measured at one point in the flow, with the magnetic field applied in the region between the dashed vertical lines. ( $\Omega_1 = 200$  rpm,  $B = 2900$  G.)

common for an  $m = 2$  mode to grow up before an  $m = 1$  dominates at saturation. High- $\Lambda$  scenarios at very slow rotation rates show that  $m$  at saturation increases as  $\Lambda$  increases. Primary mode numbers up to  $m = 5$  have been observed with  $\Lambda = 127$  at a rotation rate of 0.25 rpm.

The necessity of shear at the axial boundary has been verified experimentally. Experiments were performed with the components rotating in the standard Rayleigh-stable configuration, but with a number of different inner ring speeds. The critical magnetic field for instability varied with the differential rotation between the end cap rings as expected. When the inner rings and outer rings corotated, the instability was not observed.

The free shear layer has been measured experimentally at low Re and high  $\Lambda$  where it penetrates to the midplane of the experiment as shown in Fig. 4. The width of the layer measured at a time just before the onset of instability is consistent with the expected width scaling for a Shercliff layer  $\delta \sim 1/\sqrt{M}$ , where the Hartmann number  $M = Bl/\sqrt{4\pi\rho\eta\nu}$  and  $l = r_2 - r_1$  is a characteristic length. The onset of the instability is associated with a decrease in the mean shear in this layer.

Nonlinear numerical MHD simulations have been performed with the HERACLES code [20], modified to include finite viscosity and resistivity [21]. The simulations were performed in the experimental geometry with a  $200 \times 64 \times 400$  grid in  $\hat{r}$ ,  $\hat{\theta}$ , and  $\hat{z}$ , with  $Re = 4000$  and a range of Rm and  $M$ . These simulations show the formation of the free Shercliff layer extending from the

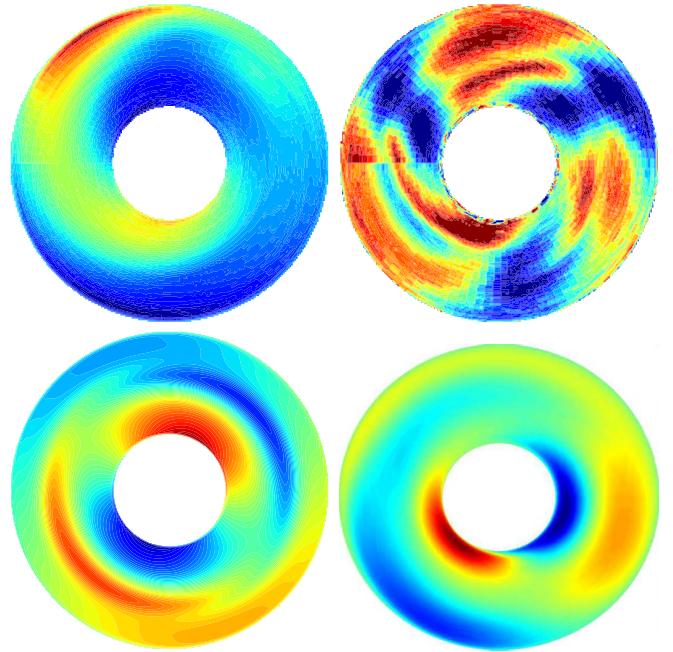


FIG. 3 (color online). Comparison of measured unstable mode with results from simulation. All are contour plots of azimuthal velocity at the midplane with the  $m = 0$  contribution subtracted. Red indicates positive velocity (counterclockwise), and blue indicates negative velocity (clockwise). Upper left: Experimental measurement with  $\Lambda = 1.4$ , reconstructed from projecting the time behavior of the azimuthal velocity as measured by one UDV transducer onto the  $r$ - $\theta$  plane. Upper right: Experimental measurement with  $\Lambda = 50$ . Lower left: Growing  $m = 1$  mode produced by a hydrodynamic linear stability analysis of an axially independent shear layer. Lower right: Unstable mode from nonlinear MHD calculation with  $Re = 4000$ ,  $Rm = 10$ , and  $\Lambda = 1$ .

discontinuity at the axial boundaries, as shown in Fig. 1. The axial length of the shear layer scales with  $\sqrt{\Lambda}$ , which seems to arise from a competition of magnetic forces, which act to extend the shear layer into the fluid, and poloidal circulation generated by the axial boundaries, which acts to disrupt the free shear layer. The simulations also produce an instability requiring  $\Lambda > 1$  for onset and suggest that a minimum penetration depth of the shear layer is required for development of the instability. Like the experimental observations, the unstable modes exhibit a spiral structure, and a cascade is observed from higher azimuthal mode number during the growth phase of the instability to a dominant  $m = 1$  at saturation.

A global linear stability analysis was performed to investigate unstable modes in the experimental geometry. The analysis found eigenvalues of the linearized nonideal MHD equations discretized across 2048 grid cells in the radial direction, assuming sinusoidal azimuthal dependence with a specified mode number and no axial dependence. Unstable hydrodynamic solutions were sought for realistic fluid parameters and for a zeroth order,

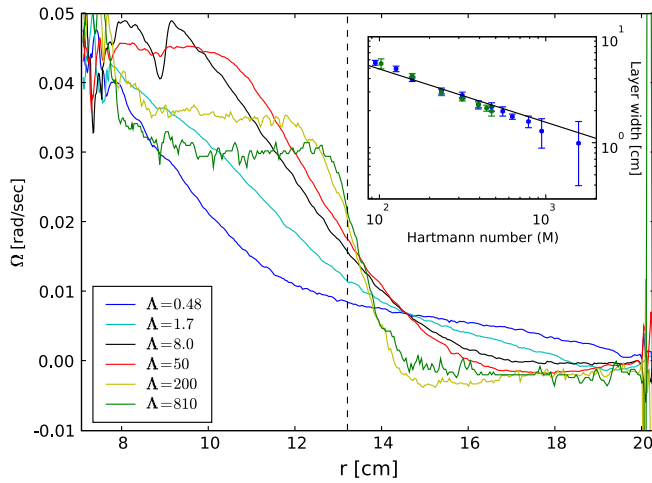


FIG. 4 (color online). Angular velocity versus radius at the midplane for several values of applied fields at a rotation rate of 0.5 rpm in the Rayleigh-unstable configuration. The dashed line indicates the radial position of the split between the axial end caps. The inset plot shows measurements of the shear layer thickness from experiments at 0.25 rpm (green) and 0.5 rpm (blue) versus the Hartmann number  $M$ .  $M = 55\sqrt{\Lambda}$  at 0.5 rpm, and  $M = 39\sqrt{\Lambda}$  at 0.25 rpm. The solid line indicates the expected Shercliff layer width scaling  $\delta \sim d/\sqrt{M}$ , where the constant  $d = 62$  cm has been chosen to match the data.

background rotation profile consisting of a free shear layer represented by a hyperbolic tangent centered between the inner and outer cylinders. Angular velocity profiles with a sufficiently narrow shear layer were found to be hydrodynamically unstable to nonaxisymmetric Kelvin-Helmholtz modes with a similar structure to those observed experimentally. The most unstable mode number increases with decreasing shear layer width, similar to the experimental observations of the saturated states.

The results presented here describe a minimum magnetic field required for onset of the instability. Simulations have shown that a sufficiently strong magnetic field will restabilize this instability, similar to the simulation results in spherical geometry [9]. Experimentally, the decreasing saturated amplitude with increasing field at small rotation rates, shown in Fig. 2, suggests that this critical field strength is being approached. But the limits on controllable slow rotation and on the availability of strong magnetic fields precluded verification of the complete restabilization.

This free-Shercliff-layer instability exhibits strong similarities to the expected behavior of the standard MRI in a Taylor-Couette device because in both cases a magnetic field acts to destabilize otherwise stable flow and in both cases the associated angular momentum transport results in a large modification to the azimuthal velocity profile. But this instability is a hydrodynamic instability on a background state established by the magnetic field and is present with  $Rm \ll 1$ . While there are inductionless relatives of the standard MRI, such as the so-called HMRI which relies on azimuthal and axial applied magnetic fields

[22,23], the unimportance of induction here is in stark contrast to the requirement of a finite minimum  $Rm$  for the standard MRI in an axial magnetic field.

These results have particular relevance to other MHD experiments in which similar shear layers may be established. A spherical Couette MHD experiment produced a nonaxisymmetric instability with applied magnetic field that was claimed to be the MRI [24]. However, subsequent simulations have attributed those observations to hydrodynamic instability of free shear layers [25,26], similar to the observations that we report. We expect that other cylindrical devices, such as the PROMISE 2 experiment [27], could produce this instability. But the critical value of  $\Lambda$  will likely change for experiments with different geometric aspect ratios.

The free-Shercliff-layer instability is not expected to impact the study of the MRI in this device since the magnetic fields required for the MRI are weaker than those required for the Shercliff layer instability at MRI-relevant speeds [21].

This work was supported by the U.S. Department of Energy's Office of Sciences—Fusion Energy Sciences Program under contract number DE-AC02-09CH11466, the U.S. National Science Foundation under grant numbers AST-0607472 and PHY-0821899, and the U.S. National Aeronautics and Space Administration (NASA) under Grant No. APRA08-0066 and No. ATP06-35.

\*aroach@pppl.gov

†hji@pppl.gov

- [1] S. A. Balbus and J. F. Hawley, *Astrophys. J.* **376**, 214 (1991).
- [2] J. Hartmann, K. Dan. Vidensk. Selsk. Mat. Fys. Medd. **15**, (1937).
- [3] J. A. Shercliff, *Math. Proc. Cambridge Philos. Soc.* **49**, 136 (1953).
- [4] K. Stewartson, *J. Fluid Mech.* **3**, 17 (1957).
- [5] B. Lehnert, *Proc. R. Soc. A* **233**, 299 (1955).
- [6] K. Stewartson, *Q. J. Mech. Appl. Math.* **10**, 137 (1957).
- [7] S. Braginskii, *Sov. Phys. JETP* **10**, 1005 (1960).
- [8] W. Liu, *Phys. Rev. E* **77**, 056314 (2008).
- [9] R. Hollerbach and S. Skinner, *Proc. R. Soc. A* **457**, 785 (2001).
- [10] R. Hollerbach, B. Futterer, T. More, and C. Egbers, *Theor. Comput. Fluid Dyn.* **18**, 197 (2004).
- [11] X. Wei and R. Hollerbach, *Phys. Rev. E* **78**, 026309 (2008).
- [12] N. Schaeffer and P. Cardin, *Phys. Fluids* **17**, 104111 (2005).
- [13] R. Hide and C. W. Titman, *J. Fluid Mech.* **29**, 39 (1967).
- [14] A. Kageyama, H. Ji, J. Goodman, F. Chen, and E. Shoshan, *J. Phys. Soc. Jpn.* **73**, 2424 (2004).
- [15] H. Ji, M. Burin, E. Schartman, and J. Goodman, *Nature (London)* **444**, 343 (2006).
- [16] E. Schartman, H. Ji, and M. J. Burin, *Rev. Sci. Instrum.* **80**, 024501 (2009).
- [17] N. B. Morley, J. Burris, L. C. Cadwallader, and M. D. Nornberg, *Rev. Sci. Instrum.* **79**, 056107 (2008).

- [18] Y. Takeda, *Nucl. Eng. Des.* **126**, 277 (1991).
- [19] UDV system manufactured by Signal Processing, S.A.
- [20] M. Gonzalez, E. Audit, and P. Huynh, *Astron. Astrophys.* **464**, 429 (2007).
- [21] C. Gissinger *et al.*, *Phys. Fluids* (to be published).
- [22] R. Hollerbach and G. Rüdiger, *Phys. Rev. Lett.* **95**, 124501 (2005).
- [23] F. Stefani, T. Gundrum, G. Gerbeth, G. Rüdiger, J. Szklarski, and R. Hollerbach, *New J. Phys.* **9**, 295 (2007).
- [24] D. R. Sisan, N. Mujica, W. A. Tilletson, Y.-M. Huang, W. Dorland, A. B. Hassam, T. M. Antonsen, and D. P. Lathrop, *Phys. Rev. Lett.* **93**, 114502 (2004).
- [25] C. Gissinger, H. Ji, and J. Goodman, *Phys. Rev. E* **84**, 026308 (2011).
- [26] R. Hollerbach, *Proc. R. Soc. A* **465**, 2003 (2009).
- [27] F. Stefani, G. Gerbeth, T. Gundrum, R. Hollerbach, J. Priede, G. Rüdiger, and J. Szklarski, *Phys. Rev. E* **80**, 066303 (2009).